Atmospheric
Chemistry
and Physics
Discussions

The size-composition distribution of atmospheric nanoparticles over Europe

David Patoulias[1,2], Christos Fountoukis[2,3], Ilona Riipinen[4], Ari Asmi[5], Markku Kulmala[5], and

Spyros N. Pandis[1,2,6]

[1] Department of Chemical Engineering, University of Patras, Patras, Greece

[2] Institute of Chemical Engineering Sciences, Foundation for Research and Technology Hellas (FORTH/ICE-HT), Patras, Greece

[3] Qatar Environment & Energy Research Institute, Hamad Bin Khalifa University, Doha, Qatar

[4] Department of Applied Environmental Science & Bert Bolin Centre for Climate Research, Stockholm University, Stockholm, Sweden

[5] Institute of Atmospheric and Earth System Research / Physics, University of Helsinki, Helsinki, Finland.

[6] Department of Chemical Engineering, Carnegie Mellon University, Pittsburgh, PA 15213, USA.

Abstract

PMCAMx-UF, a three-dimensional chemical transport model focusing on the simulation of the ultrafine particle size distribution and composition has been extended with the addition of the volatility basis set (VBS) approach for the simulation of organic aerosol (OA). The model was applied in Europe to quantify the effect of secondary semi-volatile organic vapors on particle number concentrations. The model predictions were evaluated against field observations collected during the PEGASOS-2012 campaign. The measurements included both ground and airborne measurements, from stations across Europe and a Zeppelin measuring above Po-Valley. The ground level concentrations of particles larger than 100 nm (N_{100}) were reproduced with a daily normalized mean error of 40% and a daily normalized mean bias of -20%. PMCAMx-UF tended to overestimate the concentration of particles larger than 10 nm (N_{10}) with a daily normalized mean bias of 75%. The model performed quite well compared to the Zeppelin measurements, reproducing more than 85% of N_{10} and 75% of the N_{100} data, within a factor of 2. The condensation of organics led to an increase (50-120%) of the N_{100} concentration mainly in central and northern Europe, while the N_{10} concentration decreased by 10-30%. Including the VBS in the PMCAMx-UF improved its ability to simulate aerosol number concentration compared to simulations neglecting organic condensation on ultrafine particles.

Atmospheric
Chemistry
and Physics
Discussions

1. Introduction

New particles are introduced in the atmosphere by two major processes; direct emission from multiple sources and nucleation from low volatility vapors. Nucleation and subsequent growth of new particles have been observed in a variety of environments worldwide (Kulmala et al., 2004), representing a significant source of aerosol number. Fresh particles formed by nucleation can either be lost through coagulation with pre-existing larger particles or grow through condensation of vapors (e.g. sulfuric acid, ammonia, organics, and nitric acid) to larger sizes (Adams and Seinfeld, 2002) and become cloud condensation nuclei (CCN), thereby increasing the cloud droplet number concentration (Adams and Seinfeld, 2002). Thus, nucleation and subsequent growth by condensation can be an important source of CCN (Makkonen et al., 2009; Merikanto et al., 2009; Pierce and Adams, 2009; Wang and Penner, 2009; Yu and Luo, 2009).

Considerable uncertainty arises from the partial understanding of the identity of the species involved in the growth of these nuclei (Kulmala et al., 2004; Kerminen et al., 2012). Field measurements (Eisele and McMurry, 1997; Weber et al., 1998, 1999) and model simulations (Kulmala et al., 2000; Pirjola and Kulmala, 2001; Anttila and Kerminen, 2003) indicated that the condensation of sulfuric acid alone is often not sufficient to justify the observed growth rates of fresh particles (Riipinen et al., 2011). Under some conditions, growth of new particles has been attributed to the condensation of organic species (Kulmala et al., 1998; Anttila and Kerminen, 2003; Kerminen et al., 2000), heterogeneous reactions (Zhang and Wexler, 2002), or ion-enhanced condensation (Laakso et al., 2002).

Secondary organic aerosol (SOA) comprises a major mass fraction (20-90%) of sub-micrometer particulate matter in many locations around the globe (Jimenez et al., 2009). Even though organic aerosol (OA) has been the subject of numerous studies (Hallquist et al., 2009), its chemical composition remains uncertain, making it one of the least understood components of atmospheric aerosols, due to the large number of different atmospheric organic compounds (Goldstein and Galbally, 2007).

Atmospheric OA composition continuously evolves with time as a result of various chemical reactions (Kanakidou et al., 2005). The semi-volatile products which are produced from the gas-phase oxidation of volatile organic compounds (VOCs) can afterwards condense to the particulate phase. The volatility bases set (VBS) framework describes the volatility distribution of OA compounds (Donahue et al., 2006) using logarithmically spaced bins of the

Atmospheric
Chemistry
and Physics
Discussions

64   effective saturation concentration, C^* (in µg m^{-3}) at 298 K, to classify atmospheric organic

65   species. This framework has been tested in three-dimensional regional (3-D) chemical transport

66   models (CTMs), and appears to perform well for simulations of aerosol mass distributions

67   (Gaydos et al., 2007; Karydis et al., 2007; Murphy et al., 2009; Tsimpidi et al., 2010; Fountoukis

68   et al., 2011, 2014).

69   A new 3-D CTM, PMCAMx-UF, with detailed aerosol microphysics was developed by

70   Jung et al. (2010), and has been used for simulations over the US and Europe (Fountoukis et al.,

71   2012; Baranizadeh et al., 2016). For the US domain, the first comparison of the model and the

72   measurements in Pittsburgh was encouraging; this evaluation focused on the frequency, timing,

73   and strength of nucleation events (Jung et al., 2010). Applications in Europe compared model

74   predictions against size distribution measurements from seven sites (Fountoukis et al., 2012).

75   The model was capable of reproducing more than 70% of the hourly number concentrations of

76   particles larger than 10 nm (N_{10}) within a factor of 2. However, the concentration of particles

77   larger than 100 nm (N_{100}, the number of particles that can act as CCN) was underpredicted by

78   50%. Even at sites where the sulfate to OA mass ratio was high (e.g., Melpitz), the nanoparticle

79   growth rates was underpredicted, but with smaller errors as compared with sites with relatively

80   less sulfate. These problems were caused mainly by insufficient organic vapor condensation

81   (Fountoukis et al., 2012), as the model did not explicitly include SOA condensation on ultrafine

82   particles. Based on observations from two background sites, Riipinen et al. (2011) estimated that

83   roughly half of the condensed organic mass should contribute to nanoparticle growth in order to

84   explain the observed aerosol growth rates.

85   Patoulias et al. (2015) developed a new aerosol dynamic model, DMANx (Dynamic Model

86   for Aerosol Nucleation), that simulates aerosol size/composition distribution, and includes the

87   condensation of organic vapors on nanoparticles using the VBS framework. Simulations were

88   performed for the sites of Hyytiälä (Finland) and Finokalia (Greece); two locations with different

89   organic sources. Patoulias et al. (2015) investigated the effect of condensation of organics and

90   chemical aging reactions of SOA precursors on ultrafine particle growth and particle number

91   concentration during a typical springtime nucleation event in both locations. At the Finokalia

92   site, the simulations suggested that the organics play a complementary role in new particle

93   growth, contributing 45% to the total mass of new particles. Condensation of organics increased

94   the N_{100} by 13% at Finokalia, and 25% at Hyytiälä during a typical spring day with nucleation.

Atmospheric
Chemistry
and Physics
Discussions

95   The overall objective of this work is to examine the effect of the condensation of secondary

96   organic vapors (products of the oxidation of VOCs and of the intermediate volatility organic

97   compounds; IVOCs) on particle number concentrations. Our hypothesis is that simulation of the

98   corresponding interactions improves the ability of CTMs to reproduce ambient observations of

99   the aerosol number distribution. We extended the 3-D CTM PMCAMx-UF (Fountoukis et al.,

100   2012; Jung et al., 2010), which originally assumed that ultrafine particles can grow only by

101   condensation of sulfuric acid and ammonia as well as by coagulation. The updated version of

102   PMCAMx-UF includes the condensation of organic vapors on ultrafine particles using the VBS

103   framework. We evaluated the model by comparing its predictions to surface-based high-time-

104   resolution measurements from 16 stations in Europe and airborne measurements from the

105   PEGASOS Zeppelin campaign over the Po Valley, in Italy.

106

107   **2. Model description**

108   PMCAMx-UF is a three-dimensional CTM that simulates the aerosol number size distribution, in

109   addition to the mass/composition size distribution (Jung et al., 2010; Fountoukis et al., 2012).

110   PMCAMx-UF is based on the framework of PMCAMx (Gaydos et al., 2007; Karydis et al.,

111   2007), describing the processes of horizontal and vertical advection, emissions, horizontal and

112   vertical dispersion, wet and dry deposition, aqueous and aerosol phase chemistry, as well as

113   aerosol dynamics. For the simulation of aerosol microphysics, PMCAMx-UF uses the updated

114   DMANx model of Patoulias et al. (2015), which simulates the processes of coagulation,

115   condensation/evaporation and nucleation, assuming an internally mixed aerosol. DMANx uses

116   the two-moment aerosol sectional (TOMAS) algorithm (Adams and Seinfeld, 2002; Jung et al.,

117   2006). A key feature of TOMAS is its ability to track two independent moments of the aerosol

118   size distribution for each size bin; the aerosol number and mass concentration.

119   The aerosol size distribution is discretized into 41 sections covering the diameter range

120   from approximately 0.8 nm to 10 μm. The lowest boundary is at 3.75×10^{-25} kg of dry aerosol

121   mass per particle. Each successive boundary has twice the mass of the previous one. The particle

122   components modeled include sulfate, ammonium, nitrate, sodium, chloride, crustal material,

123   water (H_2O), elemental carbon (EC), primary organic aerosol (POA) and four SOA components.

124   The TOMAS algorithm simulates the evaporation, condensation of sulfuric acid (H_2SO_4),

125   ammonia (NH_3) and organics, independently.

Atmospheric
Chemistry
and Physics
Discussions

126

2.1 Nucleation parameterizations

127

128 PMCAMx-UF has the option of using a number of nucleation treatments (Fountoukis et al.,

129 2012; Baranizadeh et al., 2016). In this work, the nucleation rate was calculated using a scaled

130 ternary nucleation parameterization based on the original expressions of Napari et al. (2002) and

131 the binary parameterization of Vehkamäki et al. (2002), if the NH_3 concentration is below a

132 threshold value of 0.01 ppt. The original NH_3-H_2SO_4-H_2O parameterization had predicted

133 successfully the presence or lack of nucleation events (Gaydos et al., 2005) in sulfur rich

134 environments. However, it overpredicted ultrafine number concentrations during nucleation

135 events (Fountoukis et al., 2012; Jung et al., 2008, 2010), and thus a scaling factor of 10^{-6} was

136 applied to the nucleation rate following the suggestions of Fountoukis et al. (2012). The critical

137 nucleus is assumed to consist of roughly two molecules of sulfuric acid and two molecules of

138 ammonia (Napari et al., 2002).

139

2.2 Gas-phase chemistry

140

141 The gas phase chemistry mechanism in PMCAMx-UF was updated in this work to the SAPRC

142 chemical mechanism (Carter, 2000; Environ, 2003), which includes 211 reactions of 56 gases

143 and 18 free radicals. The SAPRC version used here includes five lumped alkanes (ALK1-5), two

144 lumped olefins (OLE1-2), two lumped aromatics (ARO1-2), isoprene (ISOP), a lumped

145 monoterpene (TERP) and a lumped sesquiterpene species (SESQ). OLE1 contains all the

146 terminal alkenes, while OLE2 represents all the internal and cyclic alkenes. All lumped VOCs

147 with the exception of ALK1-3 are considered as SOA precursors (Lane et al., 2008; Tsimpidi et

148 al., 2010).

149

2.3 Coagulation

150

151 Coagulation of particles in the atmosphere is an important sink of aerosol number, but is also a

152 mechanism by which freshly nucleated particles grow to larger sizes (Adams and Seinfeld,

153 2002). The TOMAS algorithm is used for the simulation of coagulation. Following Adams and

154 Seinfeld (2002), TOMAS assumes that the particles coagulate via Brownian diffusion and the

155 effects of gravitational settling and turbulence are neglected.

156

Atmospheric
Chemistry
and Physics
Discussions

2.4 Particle number/mass emissions

The EUCAARI (European Integrated project on Aerosol, Cloud, Climate, and Air Quality Interactions) Pan-European anthropogenic particle number emission inventory (Kulmala et al., 2011) was used in this study. Hourly gridded anthropogenic and biogenic emissions included both gases and primary particulate matter. Three different datasets were combined in order to produce the biogenic gridded emissions for the model. Emissions from ecosystems were estimated by MEGAN (model of emissions of gases and aerosols from nature; Guenther et al., 2006). MEGAN uses as inputs the plant functional type, the leaf area index, various chemical species emission factors and weather data provided by the weather research and forecasting model (WRF) (Skamarock et al., 2005). Since sea surface covers a considerable portion of the domain, the marine aerosol emission model developed by O'Dowd et al. (2008) was also used. Wind speed fields from WRF and chlorophyll-a concentrations were used as inputs of the marine aerosol model. VOCs were speciated based on the approach proposed by Visschedijk et al. (2007). Anthropogenic gas emissions included land emissions from the GEMS (global and regional Earth-system monitoring using satellite and in-situ data) dataset (Visschedijk et al., 2007), as well as international shipping emissions. Industrial, domestic, agricultural and traffic emission sources were included in the anthropogenic inventory.

2.5 Condensation/Evaporation

Condensation of gas-phase species to existing aerosol particles is an important source of aerosol mass and a means by which small particles grow to CCN sizes. The TOMAS algorithm was used for the simulation of condensation/evaporation of sulfuric acid, ammonia and organic vapors, using the wet diameters of the particles (Gaydos et al., 2005).

Sulfuric acid is assumed to be in pseudo-steady state in DMANx. This pseudo steady-state approximation (PSSA) for sulfuric acid proposed by Pierce and Adams (2009) increases the computational speed with a small loss in accuracy. Jung et al. (2010) evaluated the performance of PSSA for sulfuric acid in DMAN against a 4th order Runge-Kutta algorithm and showed that PSSA was accurate and computationally efficient. Condensation of ammonia was simulated following the approach described by Jung et al. (2006). Ammonia condensation on the ultrafine particles ends when sulfate is fully neutralized to ammonium sulfate. Semi-volatile nitric acid and hydrochloric acid in DMAN partition to particles (as nitrate and chloride, respectively) in the

Atmospheric
Chemistry
and Physics
Discussions

188   accumulation mode range. This simplification dramatically reduces the computational burden,

189   and is not problematic for accuracy since ultrafine particle growth is governed by low volatility

190   compounds.

191

192   **2.6 Secondary organic aerosol formation**

193   Gas-phase oxidation of VOCs produces semi-volatile products that can then condense to the

194   particle phase. The VBS framework used in PMCAMx-UF (Donahue et al., 2006) describes the

195   volatility distribution of the OA compounds. SOA partitioning was simulated using 4 volatility

196   bins ($1 - 10^3$ μg m^{-3} at 298 K). We assume an average molecular weight of 200 g mol^{-1} for SOA,

197   and an effective enthalpy of vaporization of 30 kJ mol^{-1} (Pathak et al., 2007; Stanier et al., 2007).

198   The SOA yields used in the updated version of PMCAMx-UF are based on the NO_x-dependent

199   stoichiometric yields of Murphy at al. (2009). The partitioning of OA between the gas and

200   particulate phases was calculated dynamically (Patoulias et al., 2015).

201

202   **2.7 Meteorological input fields**

203   Meteorological inputs to PMCAMx-UF included horizontal wind components, vertical

204   diffusivity, temperature, pressure, water vapor, clouds and rainfall. The meteorological model

205   WRF (Skamarock et al., 2005) was used to create the above inputs. WRF was driven by

206   geographical and dynamic meteorological data (historical data generated by the Global Forecast

207   System). Each layer of PMCAMx-UF was aligned with the layers used in WRF. The WRF

208   simulation was periodically re-initialized (every 3 days) with observed conditions to ensure

209   accuracy in the corresponding fields that were used as inputs in PMCAMx-UF from June 5 to

210   July 8, 2012.

211

212   **3. Model Application and Measurements**

213   The PMCAMx-UF modeling domain in this application covered a 5400 × 5832 km^2 region in

214   Europe, with 150 cells in the x- and 162 cells in the y-direction, with a 36 × 36 km grid

215   resolution and 14 vertical layers extending up to approximately 6 km (Fig. 1). PMCAMx-UF was

216   set to perform simulations on a rotated polar stereographic map projection. The first two days of

217   each simulation were excluded from the analysis to minimize the effect of the initial conditions

218   on the results. Constant very low values have been used for the boundary conditions so that the

Atmospheric
Chemistry
and Physics
Discussions

219   predicted particle number concentrations over Europe are determined for all practical purposes

220   by the emissions and corresponding processes simulated by the model.

221   An intensive field campaign took place in Europe, as part of the Pan-European-Gas-

222   AeroSOl-climate-interaction Study (PEGASOS) project, from June 5 to July 8, 2012.

223   Measurements of aerosol size distribution from the Aerosols, Clouds, and Trace gases Research

224   Infra-Structure Network (ACTRIS), Chemistry-Aerosol Mediterranean Experiment (ChArMEx)

225   and the German Ultrafine Aerosol Network (GUAN) network are also available for the same

226   period. The model results were compared against measurements in ground sites (Fig. 1):

227   Birkenes (Norway), Hyytiala (Finland), Aspvreten (Sweden), Vavihill (Sweden), K-Puszta

228   (Hungary), Ispra (Italy), San Pietro Capofiume (Italy), Corsica (France), Patras (Greece),

229   Finokalia (Greece), Thessaloniki (Greece), Mace Head (Ireland), Hohenpeissenberg (Germany),

230   Melpitz (Germany), Waldhof (Germany) and Schneefernerhaus (Germany). The measurements

231   are available in the European Supersites for Atmospheric Aerosol Research (EUSAAR),

232   ChArMEx (charmex.lsce.ipsl.fr) and EBAS databases (ebas.nilu.no). Particle size distribution

233   measurements at all sites were made using either a Differential Mobility Particle Sizer (DMPS)

234   or a Scanning Mobility Particle Sizer (SMPS). Information about all stations can be found in the

235   Supplementary Information (SI, section S1).

236   The airborne measurements acquired by a Zeppelin were part of the PEGASOS project

237   over the Po Valley in Italy, during June 5 to July 8, 2012. The Po Valley region is situated

238   between the Alps in the north and the Apennines Mountains in the south–southwest. The

239   mountains surround the valley on three sides and strongly modify both the local and regional air

240   flow patterns in the area (Sogacheva et al., 2007). High levels of pollutants are often observed in

241   the region due to the industrial, agricultural, and other anthropogenic emissions. In addition, the

242   emissions from ship traffic on the Adriatic Sea (Hamed et al., 2007) and long-range transport

243   from central-eastern Europe are possible sources of pollutants in the region (Sogacheva et al.,

244   2007). A scanning mobility particle sizer (SMPS) was used to measure the number size

245   distribution of particles in the size range of 10 to 430 nm.

246

247

248

249

Atmospheric
Chemistry
and Physics
Discussions

Open Access

EGU

250   **4. Results**

251   **4.1 Base Case simulation**

252   Figure 2 shows the base case PMCAMx-UF predictions of ground level average number

253   concentration for all particles (N_{tot}) and for particles with diameters above 10 nm (N_{10}), 50 nm

254   (N_{50}), and 100 nm (N_{100}), during June 5 to July 8, 2012. The N_{50} and N_{100} concentrations are

255   often used as proxies for CCN-related aerosol number concentrations (Fountoukis et al., 2012).

256   The N_{10} can be directly compared against the differential mobility particle sizer (DMPS) or

257   SMPS measurements. On a domain average basis, the model predicted for the ground level N_{tot} =

258   6500 cm^{-3}, N_{10} = 3800 cm^{-3}, N_{50}= 1550 cm^{-3} and N_{100} = 520 cm^{-3} during the simulated period.

259   The spatial distributions of N_{tot} and N_{10} are quite similar, while the distributions of N_{50} and N_{100}

260   are quite different both when compared against N_{tot} and from each other. High N_{tot} and N_{10} are

261   predicted in areas with frequent nucleation events and also areas with high primary particle

262   number emissions. On the other hand, the N_{50} and N_{100} are also affected by secondary particulate

263   matter production. Highest N_{tot} concentration exceeding 20,000 cm^{-3} were predicted over

264   Bulgaria, Bosnia, southern Romania, Turkey, Germany, Poland, Holland, Portugal, northern

265   Spain, eastern UK, northern Italy, and central Russia. In contrast, the highest N_{50} and N_{100}

266   concentrations are predicted over the Mediterranean, mainly in areas near southern Spain,

267   southern Italy and Greece.

268   An additional simulation, without taking into account the condensation of organics was

269   also performed. The average fractional increase of N_x, f_{Nx}, due to the condensation of organic

270   species is defined as:

271
$$f_{Nx} = \frac{N_x(\text{with organics}) - N_x(\text{without organics})}{N_x(\text{without organics})} \quad (3.2)$$

272   where x is 10, 50, 100 nm or total.

273   Predictions of f_{Nx} are shown in Fig. 3. The average fractional changes are -0.02, -0.05, 0.15

274   and 0.33 for the N_{tot}, N_{10}, N_{50} and N_{100}, respectively. The condensation of organics was predicted

275   to decrease the total number concentration N_{tot} over most continental Europe. The largest

276   decrease was approximately 50%. This rather counterintuitive result is due to the increase of

277   both the condensation and coagulation sinks as SOA is formed. These effects dominated over the

278   faster growth of fresh nuclei or other nanoparticles to larger sizes that tend to slow down their

279   coagulation rate and increase their lifetime. In the other extreme an increase of N_{tot} of

Atmospheric
Chemistry
and Physics
Discussions

280 approximately 60% was predicted over the eastern UK. In this area organic condensation does

281 lead to higher number concentrations. The predicted N_{10} also decreased between 15-30%, due to

282 organic condensation over most of Europe. The minimum value of f_{N10} was about -0.30 over

283 Serbia, while the maximum f_{N10} was about 0.35 over eastern UK. On the other hand, the

284 condensation of organics increased the N_{50} over the whole domain. The increase was 40-80%

285 over Scandinavia and northern Russia. The condensation of semi-volatile organic vapors results

286 in an increase of N_{100} by 70-150% over northern Scandinavia and northwestern Russia according

287 to PMCAMx-UF.

288 The absolute increase in particle number concentration (ΔN_x) due to the organic

289 condensation is defined as:

290 $$\Delta N_x = N_x \text{(with organics)} - N_x \text{(without organics)} \qquad (3.3)$$

291 where x is 10, 50, 100 nm or total.

292 The N_{tot} decreased over Turkey, central and Eastern Europe, and Balkans by 2000 to 5000

293 cm^{-3} while it increased over the eastern UK by roughly 3000 cm^{-3} (Fig. S1, Supplementary

294 Information, SI). The highest reduction of N_{tot} was approximately 15000 cm^{-3} over Hungary and

295 central Turkey. The predicted ΔN_{10} over central Europe was in the range of -1000 to -3000 cm^{-3}.

296 The maximum reduction of N_{10} was equal to 3600 cm^{-3} over Hungary while its maximum

297 increase was 6500 cm^{-3} over eastern UK. The N_{50} increased due to the condensation of organics

298 species over Italy, central Russia, Holland, Ukraine, eastern Mediterranean, the coast of Algeria

299 and Spain by 500 - 2000 cm^{-3}. N_{100} increases from 300 to 800 cm^{-3} over the Mediterranean and

300 south Russia. The maximum N_{100} increase was about 2000 cm^{-3} over Malta and southern Italy.

301

302 **4.2 Evaluation of extended PMCAMx-UF**

303 The predicted daily average concentrations of particles larger than 10, 50 and 100 nm, are

304 compared to the corresponding observations in all ground stations in Fig. 4. Around 65% of the

305 observed N_{10} observations were reproduced within a factor of 2 by PMCAMx-UF, with the

306 model tending to overestimate the corresponding concentrations. The model performed even

307 better for N_{50} reproducing 80% of the measurements within a factor of 2. PMCAMx-UF

308 presented a tendency to underestimate the N_{100}, levels but still reproduced 70% of the data,

309 within a factor of 2.

Atmospheric
Chemistry
and Physics
Discussions

310   The prediction skill metrics of PMCAMx-UF, when compared against the daily average

311   measurements from the 16 stations, are summarized in Tables 1-3. The average normalized mean

312   error (NME) for N_{10} was 90% and the normalized mean bias (NMB) was 75%. The N_{10} was

313   overestimated in most locations with the exception of Hyytiala, San Pietro Capofiume, and

314   Hohenpeissenberg. The normalized mean bias was less than 30% in K-Puszta, Melpitz and

315   Patras. The model really overpredicted N_{10} (NMB>100%) in several stations in Northern Europe

316   (Aspvreten, Birkenes, Vavihill), some coastal locations (Corsica and Mace Head), two German

317   sites (Waldhod and Schneefernerhaus) and the Thessaloniki site in northern Greece. The overall

318   NMB and NME for N_{50} were 25% and 50%, respectively. The N_{50} NMB was less than 50% in 14

319   stations, with only Aspvreten and Thessaloniki being exceptions. In these 14 stations the

320   corresponding error was less than 70%. Finally, the N_{100} was underpredicted in all stations with

321   the exception of two Greek sites (Thessaloniki and Finokalia). However, this underprediction

322   was less than 30% in 9 out of the 14 sites. Overall, the NMB for N_{100} was -20% and the NME for

323   N_{100} was 40% for the simulation with organics.

324   Figure 5 and Figures S2-S4 show measured and predicted average diurnal profiles of N_{10}.

325   In Hyytiala, Patras and Hohenpeissenberg, the observed diurnal profiles of N_{10} were flat, and the

326   predicted diurnal profiles of N_{10} were close to the observations. In Melpitz and San Pietro

327   Capofiume, the observed and predicted N_{10} increased at noon due to nucleation. In K-Puszta,

328   Ispra, Birkenes, Aspvreten, Vavihill, Thessaloniki, Schneefernerhaus, Finokalia, Corsica and

329   Waldhof, the model overpredicted N_{10}.

330   One of the potential explanations for the overprediction of N_{10} is the corresponding

331   overprediction in the frequency of nucleation. Figure 6 shows the predicted and measured

332   nucleation frequency for the 16 stations during June 5 to July 8, 2012. The criteria proposed by

333   Dal Maso et al. (2005) were used for the categorization of a day as a nucleation event. The

334   nucleation frequency was defined as the ratio of the number of days characterized as nucleation

335   events to the total number of days.

336   The observed nucleation frequency varied dramatically in the 16 sites from over 90% in

337   San Pietro Capofiume to less than 10% in Patras. PMCAMx-UF reproduced this wide range (Fig.

338   6) with the predicted nucleation frequency being within 20% of the observed one in 12 out of the

339   16 stations. The model tends to overpredict nucleation frequency with the most significant errors

340   in two coastal stations in the Mediterranean (Corsica and Patras) and two stations in Scandinavia

341   (Birkenes and Aspreveten). This suggests that overpredicted nucleation frequency can explain

342   part of the N_{10} overprediction in at least three (Corsica, Birkenes and Aspreveten) out of the eight

343   stations.

344   The overprediction of N_{10} could be also due to the low surface area of the particles

345   resulting in lower condensation and coagulation rates. The capability of the existing aerosol

346   population to remove vapors and freshly formed particles can be described by the condensational

347   sinks (CS) (Dal Maso et al., 2005). The model undepredicted the measured the condensational

348   sink in most of the sites. In Corsica the model overpredicted the condensation sink, while in

349   Thessaloniki, Birkenes and Aspreveten the model is in good agreement with the measurements

350   (Fig. 7). Summarizing, the errors in N_{10} are caused by the high predicted nucleation rate at

351   Aspvreten, Birkenes, Schneefernerhaus, Thessaloniki and Vavihill and they are, at least partially,

352   due to low predicted condensation sink at Ispra, K-Puszta, Mace Head and Melpitz. At Corsica,

353   the overprediction of N_{10} is due to errors in both the predicted nucleation rates and the

354   condensation sink.

355   The average diurnal profiles of N_{100} for all sites are shown in Fig. 8 and Figures S5-S7. The

356   model reproduced satisfactorily the average observed of N_{100} in the Mediterranean (Corsica, San

357   Pietro Capofiume, Patra and Finokalia) with the exceptions of Thessaloniki, where PMCAMx-

358   UF overestimated N_{100} for the most hours of the day.

359   In northern Europe, the predicted N_{100} was in general below the observed N_{100}. The

360   maximum underprediction of N_{100} was observed in Hyytiala, Mace Head, and Melpitz. This

361   indicated that the concentration of large particles was lower than observed, and therefore the

362   condensation sink was also lower (Fig. 7). This underprediction is probably due to a combination

363   of lower primary particles emissions and lower growth rates of the particles. The low prediction

364   of organic aerosol is causing the underprediction of N_{100} in Patras and San Pietro Capofiume.

365   The ability of PMCAMx-UF to reproduce the submicrometer aerosol composition during

366   this period was similar to that of PMCAMx over the same domain both at the ground and aloft

367   (Fountoukis et al., 2011). For example, the model reproduced the average mass concentrations

368   of the major inorganic PM_1 components within 20-30% in the Po Valley stations, but tended to

369   overpredict the organic aerosol concentrations. This overprediction is probably due to our

370   assumptions about the chemical aging of the biogenic SOA. The detailed evaluation of

371   PMCAMx PM_1 mass and composition predictions during the PEGASOS campaigns and the

Atmospheric
Chemistry
and Physics
Discussions

372   sensitivity of the model to chemical aging parameterizations are presented in detail in

373   forthcoming publications.

374

4.3 Comparison to Zeppelin measurements

376   The Zeppelin measurements were taken every 3 minutes in different heights, while the model

377   predictions are every 15 minutes. To compare the results, the model output was interpolated to

378   the times of the Zeppelin measurement periods. Figure S8 shows the comparison between model

379   predictions and Zeppelin measurements of N_{10} and N_{100} (averages of 2000 points). PMCAMx-UF

380   reproduced more than 80% of the 3-minute N_{10} data of Zeppelin with in a factor of 2.

381   Figure 9 shows the predicted and observed vertical concentration profiles of particle

382   number concentrations for N_{10} and N_{100}, calculated for 80 m altitude bins, averaged over the

383   entire PEGASOS campaign. The model showed a small tendency to underpredict N_{10}, especially

384   at heights between 200 and 400 m. PMCAMx-UF reproduced very well the N_{100} concentration at

385   all heights. The average measured N_{10} at all heights was 6050 cm^{-3}, while the predicted

386   concentration was equal to 5250 cm^{-3}. The model also reproduced 75% of the N_{100} Zeppelin

387   measurements (3-minute) within a factor of 2. The measured average N_{100} at all heights was 1520

388   cm^{-3} and 1380 cm^{-3} for the extended PMCAMx-UF. The ability of the revised model to

389   reproduce reasonably well the high-time resolution (3-minute) Zeppelin measurements at

390   multiple altitudes and locations is encouraging.

391   The vertical profiles shown are averages of different flights that collected data in different

392   days and different altitudes each time. There are only a few measurements at the higher altitudes

393   and these took place in periods of relatively high concentrations. This resulted in the peak at 750

394   m in Figure 9. The model predictions are for the same periods and the same altitudes. This is the

395   reason why the model can reproduce the apparent high concentration layer.

396

4.4 Effect of SOA formation on PMCAMx-UF performance

398   The results of the simulation without SOA condensation were also compared to the

399   measurements. Including the SOA condensation reduced the NMB of N_{10} by 10%. The

400   maximum decrease of N_{10} due to organics condensation appeared at noon when nucleation

401   events took place. The maximum decrease of N_{10} due to organics condensation appeared at noon

402   when nucleation events took place. Simulation of the secondary organics reduced the NMB of

Atmospheric
Chemistry
and Physics
Discussions

403   N_{100} from -40% to -20%, and the NME from -45% to -40%. The organic condensation increased

404   the average condensation sink from 3.5×10^{-3} s^{-1} to 4.2×10^{-3} s^{-1}. The addition of organics species

405   decreased the average of N_{10} from 6550 cm^{-3} to 6060 cm^{-3} (average observed N_{10} was 3910 cm^{-3})

406   while increasing the average of N_{100} from 750 cm^{-3} to 930 cm^{-3} (average observed N_{10} was 1080

407   cm^{-3}) (Tables 1-3).

408   Simulation of organics condensation improved the average predicted N_{100} at all heights in

409   the Po Valley compared to Zeppelin measurements, by reducing the underprediction of N_{100} from

410   22% to 10% (Fig S9). The model with organics reproduced the measured N_{10} well at most

411   heights, with the exception of the heights between 200 and 400 m (Fig S10a). At all heights, the

412   predicted N_{100} with organics was closer to the measurements than the prediction of N_{100} without

413   organics (Fig S10b).

414

415   **5. Conclusions**

416   A new version of PMCAMx-UF was developed including the condensation of organic vapors on

417   ultrafine particles, using the volatility basis set framework. We evaluated the model predictions

418   against field observations collected in Europe, during June 5 to July 8, 2012. The measurements

419   included both ground stations across Europe and airborne measurements from a Zeppelin. The

420   goal of this work was to better understand the effect of condensation of semi-volatile organic

421   vapors on regional aerosol number concentration in Europe during a photochemically active

422   period.

423   Including organic condensation in PMCAMx-UF improved its ability to reproduce the

424   concentration of particles larger than 10 nm (N_{10}) at ground level. The inclusion of organics

425   decreased the NMB of N_{10} from 85% to 75% and the corresponding NME from 100% to 90%.

426   However, the revised model still tends to overpredict N_{10} for the majority of the locations. This

427   overprediction of N_{10} is due to the overprediction of nucleation in some sites and the low number

428   concentration of predicted pre-existing particles (low condensational sink) and consistently low

429   coagulation rate.

430   The N_{100} predictions by PMCAMx-UF were encouraging in most sites. The NMB of N_{100}

431   was reduced from -40% to -20% after the addition of SOA condensation while the corresponding

432   NME was reduced from 45% to 40%. This underprediction of N_{100} at all sites implies the need of

433   improvement of either the size distribution of the emissions, and/or number of pre-existing

Atmospheric
Chemistry
and Physics
Discussions

434   particles (condensation sink), and/or the addition of chemical aging of semi-volatile, and/or the

435   effect of extremely low volatility organic vapors in the model (Patoulias et al., 2015).

436   The condensation of organics decreased the predicted N_{10} concentration across Europe.

437   The condensation of organics both grew ultrafine particles and increased the probability of

438   collision of fresh particles with large particles (coagulation sink). This change dominated over

439   the faster growth of the fresh particles to larger sizes in many, but not all, locations. The larger

440   reduction of N_{10} due to organic condensation (25%) was predicted over Russia, Turkey, Eastern

441   Europe and the Balkans. The SOA condensation increased the number of particles larger than

442   100 nm (N_{100}) in all locations. This predicted increase was more than 80% in northern

443   Scandinavia and northern Russia.

444   Compared to the PEGASOS Zeppelin measurements in Po Valley, PMCAMx-UF

445   reproduced the average N_{10} with an error less than 10% and N_{100} with less than 10% at all heights

446   up to 1000 m. The model with the condensation of organics performed better than the one

447   without organics, in reproducing the observed vertical profile of both N_{10} and N_{100}. The model

448   with organics reproduced more than 85% and 75% of 3 min data of Zeppelin within a factor of 2

449   for N_{10} and N_{100}, respectively.

450

463

464

Atmospheric
Chemistry
and Physics
Discussions

6. References

465   **6. References**

466   Adams, P.J., Seinfeld, J. H.: Predicting global aerosol size distributions in general circulation
467   models, J. Geophys. Res., 107, 4370, 2002.

468   Anttila, T., Kerminen, V.: Condensational growth of atmospheric nuclei by organic vapours, J.
469   Aerosol Sci., 34, 41–61, 2003.

470   Baranizadeh, E., Murphy, B. N., Julin, J., Falahat, S., Reddington, C. L., Arola, A., Ahlm, L.,
471   Mikkonen, S., Fountoukis, C., Patoulias, D., Minikin, A., Hamburger, T., Laaksonen, A.,
472   Pandis, S. N., Vehkamäki, H., Lehtinen, K. E. J., and Riipinen, I.: Implementation of state-
473   of-the-art ternary new-particle formation scheme to the regional chemical transport model
474   PMCAMx-UF in Europe, Geosci. Model Dev., 9, 2741-2754, 2016.

475   Carter, W. P. L.: Programs and files implementing the SAPRC-99 mechanism and its associates
476   emissions processing procedures for Models-3 and other regional models, January 31,
477   2000.

478   Dal Maso, M., Kulmala M., Riipinen, I., Wagner, R., Hussein, T., Aalto, P. and Lehtinen, K. E.
479   J.: Formation and growth of fresh atmospheric aerosols: eight years of aerosol size
480   distribution data from SMEAR II, Hyytiälä, Finland, Boreal Env. Res., 10, 323–336, 2005.

481   Donahue, N. M., Robinson, A. L., Stanier, C. O., and Pandis, S. N.: Coupled partitioning,
482   dilution, and chemical aging of semivolatile organics, Environ. Sci. Technol., 40, 2635–
483   2643, 2006.

484   Eisele, F. L. and McMurry, P. H.: Recent progress in understanding particle nucleation and
485   growth, Phil. Trans. Royal Soc. London, 191-201, 1997.

486   Environ, User's guide to the comprehensive air quality model with extensions (CAMx), version
487   4.02, report, ENVIRON Int. Corp., Novato, CA, 2003.

488   Fountoukis, C., Megaritis, A. G., Skyllakou, K., Charalampidis, P. E., Pilinis, C., Denier van der
489   Gon, H. A. C., Crippa, M., Canonaco, F., Mohr., C., Prévôt, A. S. H., Allan, J. D., Poulain,
490   L., Petäjä, T., Tiitta, P., Carbone, S., Kiendler-Scharr, A., Nemitz, E., O'Dowd, C.,
491   Swietlicki, E., and Pandis, S.N.: Organic aerosol concentration and composition over
492   Europe: Insights from comparison of regional model predictions with aerosol mass
493   spectrometer factor analysis, Atmos. Chem. Phys., 14, 9061 - 9076, 2014.

494   Fountoukis, C., Riipinen, I., Denier van der Gon, H. A. C., Charalampidis, P. E., Pilinis, C.,
495   Wiedensohler, A., O'Dowd, C., Putaud, J. P., Moerman, M., and Pandis, S. N.: Simulating

496   ultrafine particle formation in Europe using a regional CTM: contribution of primary

497   emissions versus secondary formation to aerosol number concentrations, Atmos. Chem.

498   Phys., 12, 8663-8677, 2012.

499 Fountoukis, C., Racherla, P. N., Denier van der Gon, H. A. C., Polymeneas, P., Charalampidis,

500   P. E., Pilinis, C., Wiedensohler, A., Dall'Osto, M., O'Dowd, C., and Pandis, S. N.:

501   Evaluation of a three-dimensional chemical transport model (PMCAMx) in the European

502   domain during the EUCAARI May 2008 campaign, Atmos. Chem. Phys., 11, 10331–

503   10347, 2011.

504 Gaydos, T., Pinder, R., Koo, B., Fahey, K., Yarwood, G., and Pandis, S. N.: Development and

505   application of a three-dimensional Chemical Transport Model, PMCAMx, Atmos.

506   Environ., 41, 2594–2611, 2007.

507 Gaydos, T.M., Stainer, C.O., Pandis, S.N.: Modeling of insitu ultrafine atmospheric particle

508   formation in the eastern United State, J. Geophys. Res., 110, D07S12,

509   doi:10.1029/2004JD004683, 2005.

510 Goldstein, A. H. and Galbally, I. E.: Known and unexplored organic constituents in the earth's

511   atmosphere, Environ. Sci. Technol., 41, 1514–1521, 2007.

512   Guenther, A., Karl, T., Harley, P., Wiedinmyer, C., Palmer, P. I., and Geron, C.: Estimates of

513   global terrestrial isoprene emissions using MEGAN (Model of Emissions of Gases and

514   Aerosols from Nature), Atmos. Chem. Phys., 6, 3181–3210, 2006.

515 Hallquist, M., Wenger, J. C., Baltensperger, U., Rudich, Y., Simpson, D., Claeys, M., Dommen,

516   J., Donahue, N. M., George, C., Goldstein, A. H., Hamilton, J. F., Herrmann, H.,

517   Hoffmann, T., Iinuma, Y., Jang, M., Jenkin, M. E., Jimenez, J. L., Kiendler-Scharr, A.,

518   Maenhaut, W., McFiggans, G., Mentel, T. F., Monod, A., Prevot, A. S. H., Seinfeld, J. H.,

519   Surratt, J. D., Szmigielski, R., and Wildt, J.: The formation, properties and impact of

520   secondary organic aerosol: current and emerging issues, Atmos. Chem. Phys., 9, 5155–

521   5236, 2009.

522 Hamed, A., Joutsensaari, J., Mikkonen, S., Sogacheva, L., Dal Maso, M., Kulmala, M., Cavalli,

523   F., Fuzzi, S., Facchini, M. C., Decesari, S., Mircea, M., Lehtinen, K. E. J., and Laaksonen,

524   A.: Nucleation and growth of new particles in Po Valley, Italy, Atmos. Chem. Phys., 7,

525   355-376, 2007.

Atmospheric
Chemistry
and Physics
Discussions

526   Jimenez, J. L., Canagaratna, M. R., Donahue, N. M., Prevot, A. S. H., Zhang, Q., Kroll, J. H.,
527   DeCarlo, P. F., Allan, J. D., Coe, H., Ng, N. L., Aiken, A. C., Docherty, K. S., Ulbrich, I.
528   M., Grieshop, A. P., Robinson, A. L., Duplissy, J., Smith, J. D., Wilson, K. R., Lanz, V.
529   A., Hueglin, C., Sun, Y. L., Tian, J., Laaksonen, A., Raatikainen, T., Rautiainen, J.,
530   Vaattovaara, P., Ehn, M., Kulmala, M., Tomlinson, J. M., Collins, D. R., Cubison, M. J., E,
531   Dunlea, J., Huffman, J. A., Onasch, T. B., Alfarra, M. R., Williams, P. I., Bower, K.,
532   Kondo, Y., Schneider, J., Drewnick, F., Borrmann, S., Weimer, S., Demerjian, K., Salcedo,
533   D., Cottrell, L., Griffin, R., Takami, A., Miyoshi, T., Hatakeyama, S., Shimono, A., Sun, J.
534   Y., Zhang, Y. M., Dzepina, K., Kimmel, J. R., Sueper, D., Jayne, J. T., Herndon, S. C.,
535   Trimborn, A. M., Williams, L. R., Wood, E. C., Middlebrook, A. M., Kolb, C. E.,
536   Baltensperger, U., and Worsnop, D. R.: Evolution of organic aerosols in the atmosphere,
537   Science, 326, 1525–1529, 2009.
538   Jung, J., Fountoukis, C., Adams, P. J., and Pandis, S. N.: Simulation of in situ ultrafine particle
539   formation in the eastern United States using PMCAMx-UF, J. Geophys. Res., 115,
540   D03203, doi: 10.1029/2009JD012313, 2010.
541   Jung, J., Adams, P. J., and Pandis, S. N.: Evaluation of nucleation theories in a sulfur-rich
542   environment, Aerosol Sci. Technol., 42, 495–504, 2008.
543   Jung, J., Adams, P. J., and Pandis, S. N.: Simulating the size distribution and chemical
544   composition of ultrafine particles during nucleation events, Atmos. Environ., 40, 2248–
545   2259, 2006.
546   Kanakidou, M., Seinfeld, J. H., Pandis, S. N., Barnes, I., Dentener, F. J., Facchini, M. C., Van
547   Dingenen, R., Ervens, B., Nenes, A., Nielsen, C. J., Swietlicki, E., Putaud, J. P., Balkanski,
548   Y., Fuzzi, S., Horth, J., Moortgat, G. K., Winterhalter, R., Myhre, C. E. L., Tsigaridis, K.,
549   Vignati, E., Stephanou, E. G., and Wilson, J.: Organic aerosol and global climate
550   modelling: a review, Atmos. Chem. Phys., 5, 1053–1123, 2005.
551   Karydis, V. A., Tsimpidi, A. P., and Pandis, S. N.: Evaluation of a three-dimensional chemical
552   transport model (PMCAMx) in the eastern United States for all four seasons, J. Geophys.
553   Res., 112, doi: 10.1029/2006JD007890, 2007.
554   Kerminen, V.-M., Virkkula, A., Hillamo, R., Wexler, A. S., and Kulmala, M.: Secondary
555   organics and atmospheric cloud condensation nuclei production, J. Geophys. Res., 105,
556   9255–9264, 2000.

Atmospheric
Chemistry
and Physics
Discussions

Open Access

EGU

557   Kulmala, M., Toivonen, A., Makela, J. M., and Laaksonen A.: Analysis of the growth of
558   nucleation mode particles observed in Boreal forest, Tellus B, 50, 449-462, 1998.

559   Kulmala, M., Pirjola, L., Makela, J.M.: Stable sulphate clusters as a source of new atmospheric
560   particles, Nature, 404, 66–69, 2000.

561   Kulmala, M., Vehkamaki, H., Petaja, T., Dal Maso, M., Lauri, A., Kerminen, V.-M., Birmili, W.,
562   and McMurry, P. H.: Formation and growth of ultrafine atmospheric particles: A review of
563   observations, J. Aerosol Sci., 35, 143–176, 2004.

564   Kulmala, M., Asmi, A., Lappalainen, H. K., Baltensperger, U., Brenguier, J. L., Facchini, M. C.,
565   Hansson, H. C., Hov, O'Dowd, C. D., Pöschl, U., Wiedensohler, A., Boers, R., Boucher,
566   O., De Leeuw, G., Denier Van Der Gon, H. A. C., Feichter, J., Krejci, R., Laj, P.,
567   Lihavainen, H., Lohmann, U., McFiggans, G., Mentel, T., Pilinis, C., Riipinen, I., Schulz,
568   M., Stohl, A., Swietlicki, E., Vignati, E., Alves, C., Amann, M., Ammann, M., Arabas, S.,
569   Artaxo, P., Baars, H., Beddows, D. C. S., Bergström, R., Beukes, J. P., Bilde, M.,
570   Burkhart, J. F., Canonaco, F., Clegg, S. L., Coe, H., Crumeyrolle, S., D'Anna, B.,
571   Decesari, S., Gilardoni, S., Fischer, M., Fjaeraa, A. M., Fountoukis, C., George, C.,
572   Gomes, L., Halloran, P., Hamburger, T., Harrison, R. M., Herrmann, H., Hoffmann, T.,
573   Hoose, C., Hu, M., Hyvärinen, A., Hõrrak, U., Iinuma, Y., Iversen, T., Josipovic, M.,
574   Kanakidou, M., Kiendler-Scharr, A., Kirkevåg, A., Kiss, G., Klimont, Z., Kolmonen, P.,
575   Komppula, M., Kristjánsson, J. E., Laakso, L., Laaksonen, A., Labonnote, L., Lanz, V. A.,
576   Lehtinen, K. E. J., Rizzo, L. V., Makkonen, R., Manninen, H. E., McMeeking, G.,
577   Merikanto, J., Minikin, A., Mirme, S., Morgan, W. T., Nemitz, E., O'Donnell, D., Panwar,
578   T. S., Pawlowska, H., Petzold, A., Pienaar, J. J., Pio, C., Plass-Duelmer, C., Prévôt, A. S.
579   H., Pryor, S., Reddington, C. L., Roberts, G., Rosenfeld, D., Schwarz, J., Seland, O., et al.:
580   General overview: European Integrated project on Aerosol Cloud Climate and Air Quality
581   interactions (EUCAARI)-integrating aerosol research from nano to global scales, Atmos.
582   Chem. Phys., 11, 13061–130143, 2011.

583   Laakso, L., Makela, J. M., Pirjola, L., and Kulmala, M.: Model studies on ion – induced
584   nucleation in the atmosphere, J. Geophys. Res., 107, 4427, doi: 10.1029/2002JD002140,
585   2002.

Atmospheric
Chemistry
and Physics
Discussions

586   Lane, T. E., Donahue, N. M., Pandis, S. N.: Simulating secondary organic aerosol formation
587   using the volatility basis-set approach in a chemical transport model, Atmos. Environ., 42,
588   7439– 7451, 2008a.

589   Lane, T. E., Donahue, N. M., Pandis, S. N.: Effect of NOx on secondary organic aerosol
590   concentrations, Environ. Sci. Technol., 42, 6022–6027, 2008b.

591   Makkonen, R., Asmi, A., Korhonen, H., Kokkola, H., Jarvenoja, S., Raisanen, P., Lehtinen, K. E.
592   J., Laaksonen, A., Kerminen, V.- M., Jarvinen, H., Lohmann, U., Bennartz, R., Feichter, J.,
593   and Kulmala, M.: Sensitivity of aerosol concentrations and cloud properties to nucleation
594   and secondary organic distribution in ECHAM5-HAM global circulation model, Atmos.
595   Chem. Phys., 9, 1747–1766, 2009.

596   Merikanto, J., Spracklen, D. V., Mann, G. W., Pickering, S. J., and Carslaw, K. S.: Impact of
597   nucleation on global CCN, Atmos. Chem. Phys., 9, 8601–8616, 2009.

598   Murphy, B. N. and Pandis, S.N.: Simulating the formation of semivolatile primary and secondary
599   organic aerosol in a regional chemical transport model, Environ. Sci. Technol., 43, 4722–
600   4728, 2009.

601   Napari, I., Noppel, M., Vehkamaki, H., and Kulmala, M.: Parameterization of ternary nucleation
602   rates for H_2SO_4-NH_3-H_2O vapors, J. Geophys. Res., 107, doi: 10.1029/2002JD002132,
603   2002.

604   Odum, J. R., Hoffman, T., Bowman, F., Collins, D., Flagan, R. C., Seinfeld, J. H.: Gas/particle
605   partitioning and secondary organic aerosol yields. Environ. Sci. Technol., 30, 2580–2585,
606   1996.

607   Pathak, R. K., Presto, A. A., Lane, T. E., Stanier, C. O., Donahue, N. M., Pandis, S. N.:
608   Ozonolysis of a-pinene: parameterization of secondary organic aerosol mass fraction,
609   Atmos. Chem. Phys., 7, 3811–3821, 2007.

610   Patoulias, D., Fountoukis, C., Riipinen, I., and Pandis, S. N.: The role of organic condensation on
611   ultrafine particle growth during nucleation events, Atmos. Chem. Phys., 15, 6337-6350,
612   2015.

613   Pierce, J. R. and Adams, P. J.: A computationally efficient aerosol nucleation/condensation
614   method: Pseudo-steady state sulfuric acid, Aerosol Sci. Technol., 43, 216–226, 2009.

615   Pirjola, L. and Kulmala, M.: Development of particle size and composition distributions with a
616   novel aerosol dynamics model, Tellus B, 53, 491–509, 2001.

Atmospheric
Chemistry
and Physics
Discussions

617   Riipinen, I., Pierce, J. R., Yli-Juuti, T., Nieminen, T., Hakkinen, S., Ehn, M., Junninen, H.,
618   Lehtipalo, K., Petaja, T., Slowik, J., Chang, R., Shantz, N. C., Abbatt, J., Leaitch, W. R.,
619   Kerminen, V.-M., Worsnop, D. R., Pandis, S. N., Donahue, N. M., and Kulmala, M.:
620   Organic condensation: a vital link connecting aerosol formation to cloud condensation
621   nuclei (CCN) concentrations, Atmos. Chem. Phys., 11, 3865–3878, 2011.
622   Skamarock, W. C., Klemp, J. B., Dudhia, J., Gill, D. O., Barker, D. M., Wang,W., and Powers, J.
623   G.: A Description of the Advanced Research WRF Version 2, NCAR Technical Note
624   (http://www.mmm.ucar.edu/wrf/users/docs/arw v2.pdf), 2005.
625   Sogacheva, L., Hamed, A., Facchini, M. C., Kulmala, M., and Laaksonen, A.: Relation of air
626   mass history to nucleation events in Po Valley, Italy, using back trajectories analysis,
627   Atmos. Chem. Phys., 7, 839-853, 2007.
628   Stanier, C. O., Pathak, R. K., and Pandis, S. N.: Measurements of the volatility of aerosols from
629   α-pinene ozonolysis, Environ. Sci. Technol., 41, 2756–2763, 2007.
630   Tsimpidi, A. P., Karydis, V. A., Zavala, M., Lei, W., Molina, L., Ulbrich, I. M., Jimenez, J. L.,
631   and Pandis, S. N.: Evaluation of the volatility basis-set approach for the simulation of
632   organic aerosol formation in the Mexico City metropolitan area, Atmos. Chem. Phys., 10,
633   525-546, 2010.
634   Vehkamaki, H., Kulmala, M., Napari, I., Lehtinen, K. E. J., Timmreck, C., Noppel, M., and
635   Laaksonen, A.: An improved parameterization for sulfuric acid-water nucleation rates for
636   tropospheric and stratospheric conditions, J. Geophys. Res., 107, 4622–4632, 2002.
637   Visschedijk, A. J. H., Zandveld, P., and Denier van der Gon, H. A. C.: TNO Report 2007 A-
638   R0233/B: A high resolution gridded European emission database for the EU integrated
639   project GEMS, Netherlands, Organization for Applied Scientific Research, 2007.
640   Weber, R. J., McMurry, P. H., Mauldin, L., Tanner, D. J., Eisele, F. L., Brechtel, F. J.,
641   Kreidenweis, S. M., Kok, G. L., Schillawski, R. D., and Baumgardner, D.: A study of new
642   particle formation and growth involving biogenic and trace gas species measured during
643   ACE 1, J. Geophys. Res., 103, 16385–16396, 1998.
644   Weber, R. J., McMurry, P. H., Mauldin III, R. L., Tanner, D. J., Eisele, F. L., Clarke, A. D., and
645   Kapustin, V. N.: New particle formation in the remote troposphere: a comparison of
646   observations at various sites, Geophys. Res. Lett., 26, 307–310, 1999.

Atmospheric
Chemistry
and Physics
Discussions

647   Yu, F. and Luo, G.: Simulation of particle size distribution with a global aerosol model:
648   contribution of nucleation to aerosol and CCN number concentrations, Atmos. Chem.
649   Phys., 9, 7691– 7710, 2009.
650   Zhang, K.M., Wexler, A.S.: A hypothesis for condensation of fresh atmospheric nuclei, J.
651   Geophys. Res., 107, 4577, 2002.
652
653
654
655
656
657
658
659

Atmospheric
Chemistry
and Physics
Discussions

Open Access

660 **Table 1:** Prediction skill metrics of PMCAMx-UF against daily ground measurements of particle

661 number concentration with diameter above 10 nm from 16 stations during 5 June – 8 July 2012.

Station	Mean Observed	Mean Predicted (cm^{-3})		Normalized Mean Bias (NMB) (%)		Normalized Mean Error (NME) (%)	
		With Organics	Without Organics	With Organics	Without Organics	With Organics	Without Organics
N_{10}							
ASP	2090	5533	5496	165	163	165	163
BIR	1937	4950	4608	156	138	160	143
COR	2994	6768	7455	126	149	126	149
FIN	3932	6091	6191	55	57	57	60
HOH	3809	3801	4155	0	9	36	40
HYY	2616	2239	2408	-14	-8	33	35
ISP	6307	10481	11420	66	81	78	91
KPU	5245	6686	8581	27	64	56	82
MAC	822	1965	1758	139	114	149	135
MEL	6045	7325	8680	21	44	60	75
PAT	4858	5333	5449	10	12	50	53
SCH	1286	2913	3279	127	155	127	155
SPC	8319	7398	8547	-11	3	34	33
THE	4022	9755	10334	143	157	143	160
VAV	3230	7561	7601	134	135	136	137
WAL	5036	8194	8852	63	76	74	85
ALL	**3909**	**6062**	**6551**	**75**	**85**	**90**	**100**

662

663

664

665

666

667

668

Atmospheric
Chemistry
and Physics
Discussions

669   **Table 2:** Prediction skill metrics of PMCAMx-UF against daily ground measurements of particle

670   number concentration with diameter above 50 nm from 16 stations during 5 June – 8 July 2012.

Station	Mean Observed	Mean Predicted (cm^{-3})		Normalize Mean Bias (NMB) (%)		Normalized Mean Error (NME) (%)	
		With Organics	Without Organics	With Organics	Without Organics	With Organics	Without Organics
N_{50}							
ASP	1353	2419	1835	79	36	81	47
BIR	1046	1364	1111	30	6	61	53
COR	2460	3155	2883	28	17	41	37
FIN	3085	4163	3905	35	27	39	32
HOH	1988	1550	1340	-22	-33	31	35
HYY	1546	1092	829	-29	-46	40	49
ISP	3500	5399	4728	54	35	70	56
KPU	2955	3674	3424	24	16	30	25
MAC	489	315	278	-36	-43	70	67
MEL	2243	2197	1824	-2	-19	23	24
PAT	3249	3211	2983	-1	-8	29	28
SCH	839	1202	1053	43	26	65	54
SPC	3235	3686	3300	14	2	29	23
THE	2334	5147	4545	120	95	120	95
VAV	1628	2192	1812	35	11	45	33
WAL	2050	2295	1882	12	-8	22	16
ALL	**2125**	**2691**	**2358**	**25**	**10**	**50**	**40**

671

672

673

674

675

676

677

678 **Table 3:** Prediction skill metrics of PMCAMx-UF against daily ground measurements of particle

679 number concentration with diameter above 100 nm from 16 stations during 5 June – 8 July 2012.

Station	Mean Observed	Mean Predicted (cm^{-3})		Normalize Mean Bias (NMB) (%)		Normalized Mean Error (NME) (%)	
		With Organics	Without Organics	With Organics	Without Organics	With Organics	Without Organics
N_{100}							
ASP	540	372	343	-31	-37	45	46
BIR	431	318	229	-26	-47	59	55
COR	1304	1180	914	-9	-30	37	36
FIN	1769	2002	1652	13	-7	29	22
HOH	911	558	448	-40	-50	43	51
HYY	736	309	207	-60	-70	60	70
ISP	1766	1461	1245	-17	-30	32	37
KPU	1526	1486	1228	-3	-20	28	25
MAC	242	116	86	-50	-64	60	65
MEL	998	671	484	-33	-51	38	51
PAT	1758	1471	1154	-16	-34	25	35
SCH	496	442	360	-11	-27	43	36
SPC	1667	1387	1132	-17	-32	31	37
THE	1398	2020	1649	45	18	53	40
VAV	749	438	358	-41	-52	46	54
WAL	924	577	464	-38	-50	39	50
ALL	**1076**	**926**	**747**	**-20**	**-40**	**40**	**45**

680 $$\text{NMB}=\sum_{i=1}^{n}(P_i - O_i)\Bigg/\sum_{i=1}^{n}O_i \; ; \quad \text{NME}=\sum_{i=1}^{n}|P_i - O_i|\Bigg/\sum_{i=1}^{n}O_i$$

681

682
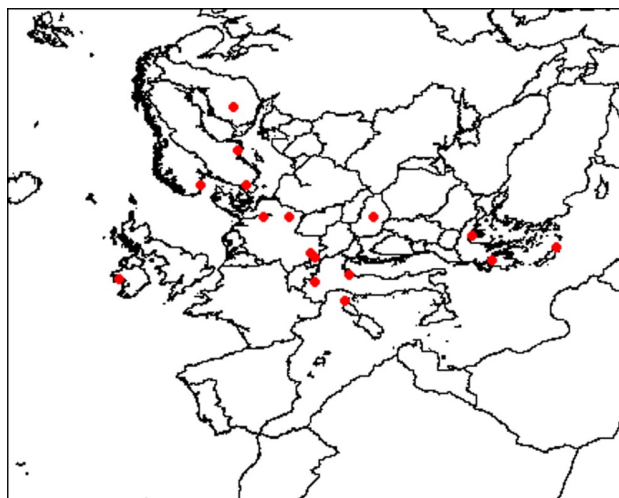
Figure 1: Modeling domain of PMCAMx-UF for Europe. Red dots show the measurement stations of Birkenes (Norway), Hyytiala (Finland), K-Puszta (Hungary), Aspvreten (Sweden), Vavihill (Sweden), Ispra (Italy), San Pietro Capofiume (Italy), Corsica (France), Patras (Greece), Finokalia (Greece), Thessaloniki (Greece), Mace Head (Ireland), Schneefernerhaus (Germany), Hohenpeissenberg (Germany), Melpitz (Germany) and Waldhof (Germany).

Atmospheric
Chemistry
and Physics
Discussions
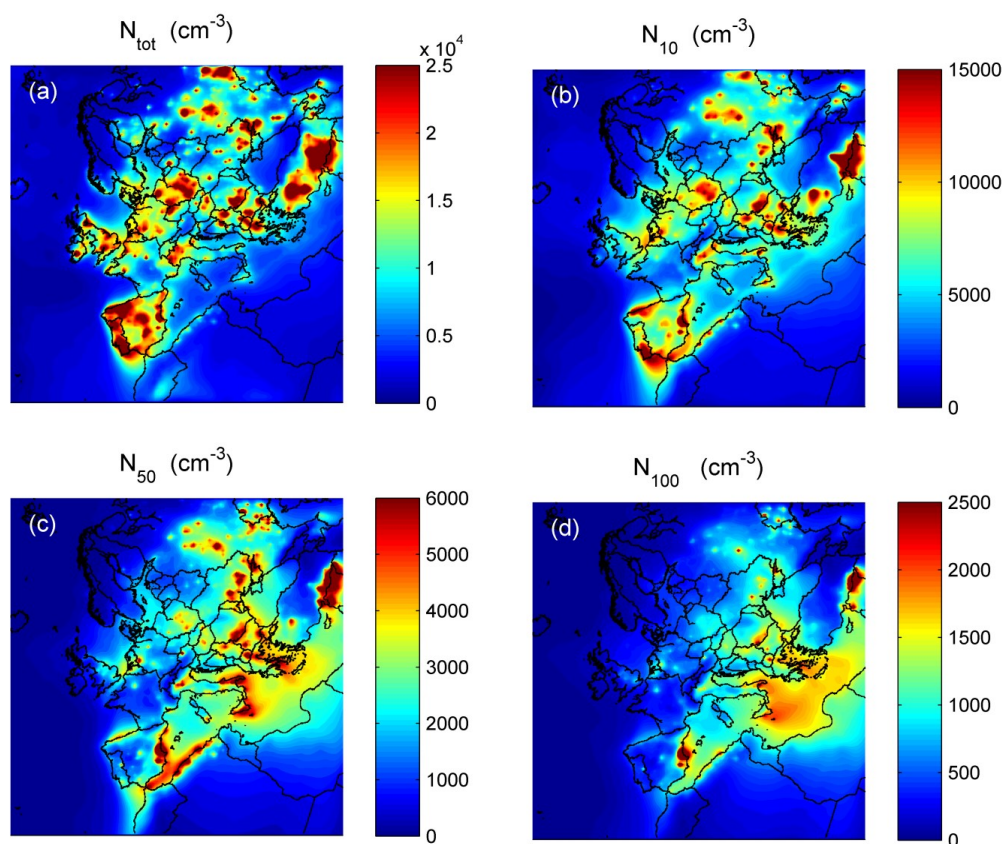
Figure 2: Ground level average number concentrations (cm^{-3}) predicted by the base case simulation during 5 June – 8 July 2012 for: (a) all particles (N_{tot}); and particles above (b) 10 nm (N_{10}); (c) 50 nm (N_{50}); and (d) 100 nm (N_{100}). Different color scales are used.
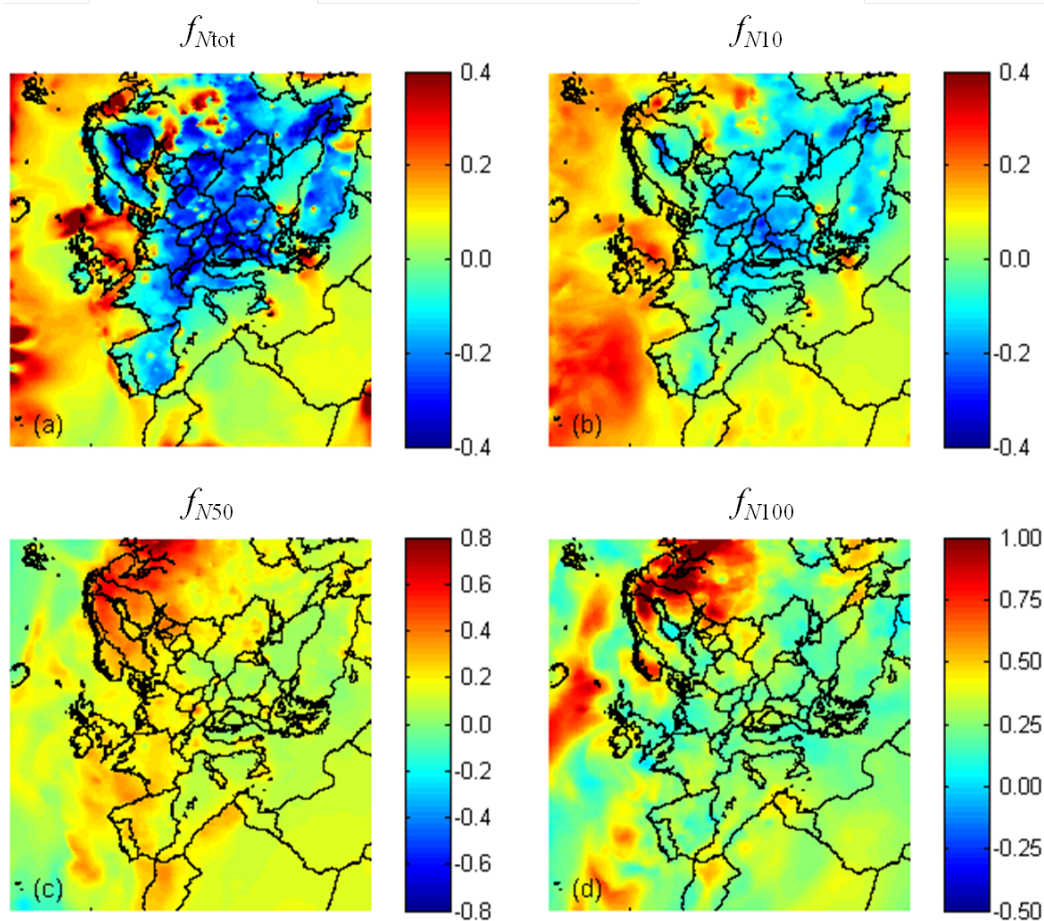
697

698

699 **Figure 3:** Ground level average fractional increase (f_{Nx}) of number concentration due to the

700 condensation of organic species predicted during 5 June – 8 July for: (a) all particles (f_{Ntot});

701 particles above (b) 10 nm (f_{N10}); (c) 50 nm (f_{N50}); and (d) 100 nm (f_{N100}). Different scales are

702 used.

703

704
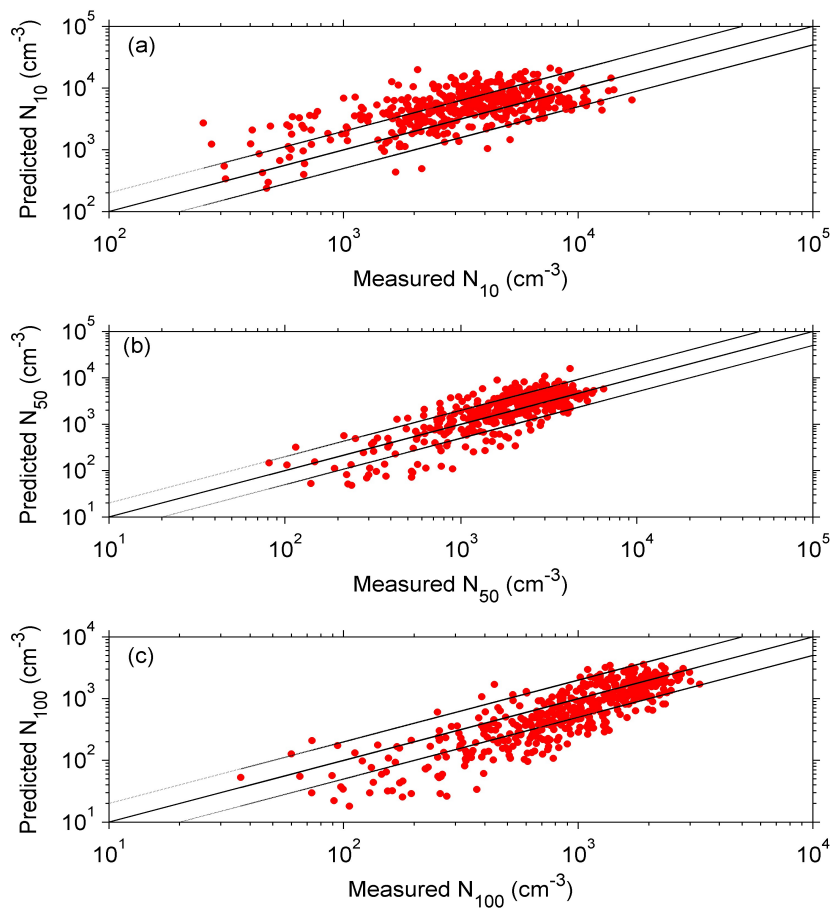
Figure 4: Comparison of predicted versus observed particle number concentrations (cm^{-3}) above

10, 50 and 100 nm from the 16 measurement stations across Europe during 5 June – 8 July 2012.

Each point corresponds to a daily average value. Also shown the 1:1, 2:1 and 1:2 lines.

708

709

710

711

712

713

714

Atmospheric
Chemistry
and Physics
Discussions

715

716
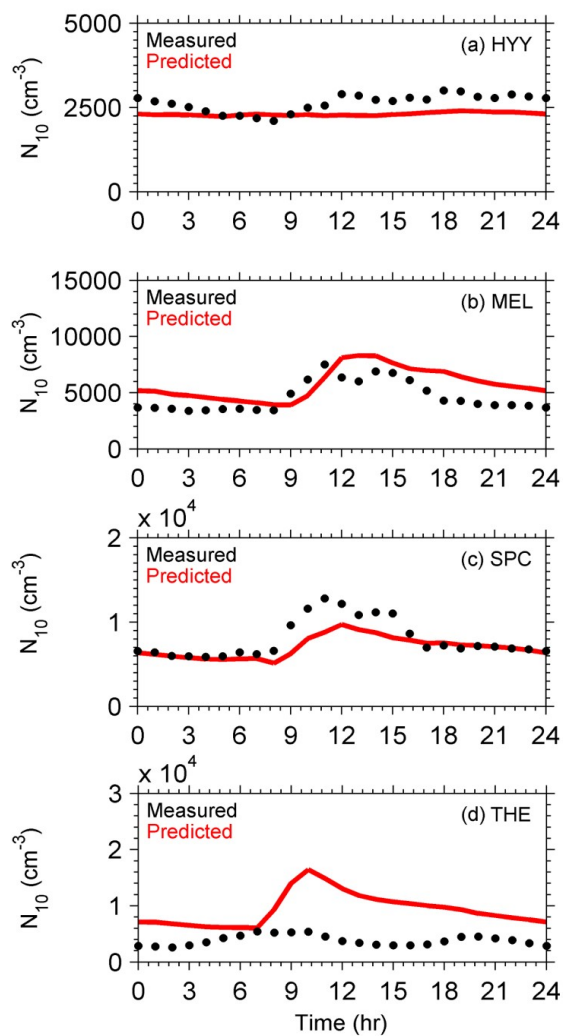
Figure 5: Average diurnal profiles of particle number concentrations (cm^{-3}) above 10 nm in: (a)

Hyytiala (Finland); (b) Melpitz (Germany); (c) San Pietro Capofiume (Italy) and (d)

Thessaloniki (Greece) during 5 June – 8 July 2012. Red lines correspond to predictions and black

symbols to observations.

721
722
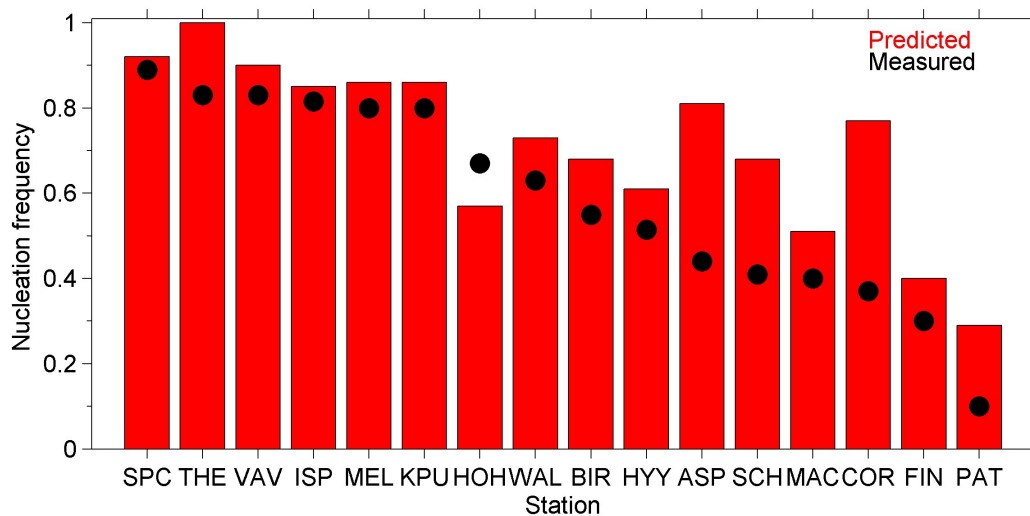
Figure 6: Predicted (red bars) vs. observed (black symbols) nucleation frequencies in the 16
measurement stations during 5 June – 8 July 2012.

725
726
727
728
729
730
731
732

Atmospheric
Chemistry
and Physics
Discussions

733

734
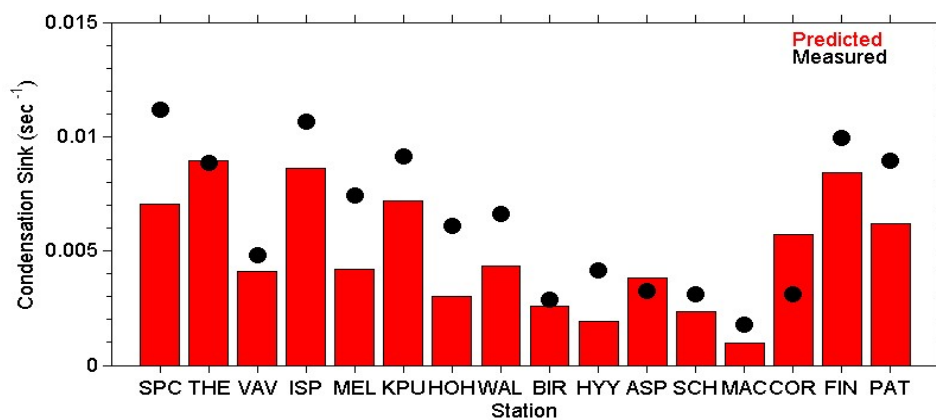
Figure 7: Predicted (red bars) vs. observed (black symbols) condensation sink in the 16

measurement stations during 5 June – 8 July 2012.

737

738
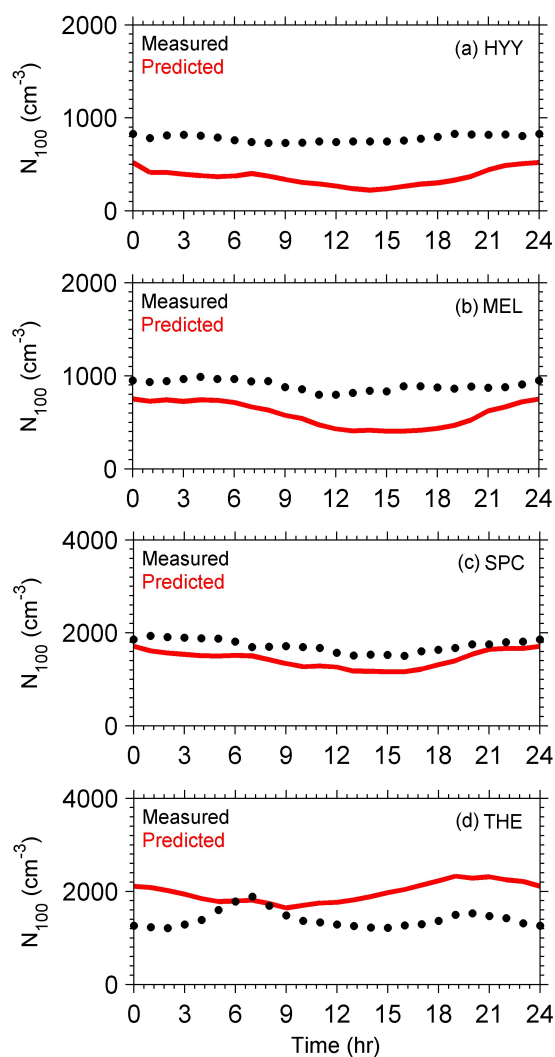
Figure 8: Average diurnal profiles of particle number concentrations (cm^{-3}) above 100 nm: in

(a) Hyytiala (Finland); (b) Corsica (France); (c) and (d) Ispra (Italy) during 5 June – 8 July 2012.

Red lines correspond to predictions and black symbols to observations.

742

743

744

745

746

747

748
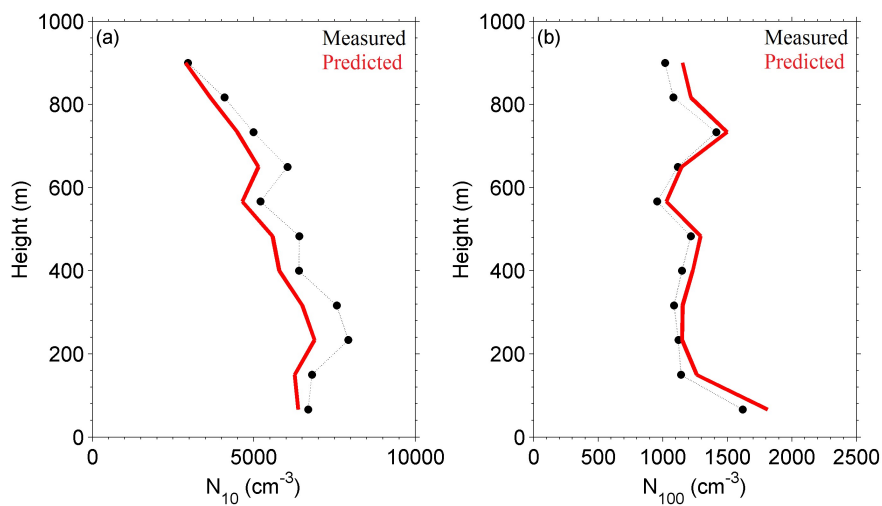
Figure 9: Comparison of predicted PMCAMx-UF (red line) vs. observed (black dots) vertical
profiles of averaged particle number concentrations for (a) N_{10} and (b) N_{100} of 25 flights over the
Po Valley during the PEGASOS campaign.

752

753